ELSEVIER

International Journal of Mass Spectrometry 202 (2000) 91–109

International Journal of Mass Spectrometry

Chemical ionization mass spectrometer for long-term measurements of atmospheric OH and H_2SO_4

H. Berresheim[a,*], T. Elste[a], C. Plass-Dülmer[a], F.L. Eisele[b,1], D.J. Tanner[b,2]

[a]*German Weather Service, Meteorological Observatory, Hohenpeissenberg, Germany*
[b]*Atmospheric Chemistry Division, National Center for Atmospheric Research, Boulder, Colorado, USA*

Received 7 December 1999; accepted 3 March 2000

Abstract

An atmospheric pressure/chemical ionization mass spectrometer (AP/CIMS) has been developed for continuous long-term measurements of atmospheric OH and H_2SO_4. The corresponding methods both involve chemical ionization of H_2SO_4 by NO_3^- ions with OH being first titrated by excess SO_2 to form equivalent concentrations of H_2SO_4 in the system. The chemical ionization mass spectrometry (CIMS) system has been operated since April 1998 at the Meteorological Observatory Hohenpeissenberg, a mountain research station of the German Weather Service in South Germany. A technical description of the apparatus is presented followed by a detailed estimate of uncertainties in calibration and ambient air measurements resulting from changes in instrumental and/or ambient parameters. Examples from both calibration runs and ambient air measurements are shown. For the present system and operating conditions accuracy, precision, and detection limit are estimated to be 39%, 30%, and 3×10^4 molecules cm^{-3} for H_2SO_4, and 54%, 48%, and 5×10^5 molecules cm^{-3} for OH measurements, respectively, based on 5 min signal integration. (Int J Mass Spectrom 202 (2000) 91–109) © 2000 Elsevier Science B.V.

Keywords: Chemical ionization mass spectrometry (CIMS); OH radical; H_2SO_4; Long-term atmospheric measurements; System performance; Error estimates

1. Introduction

The hydroxyl radical, OH, is the most important oxidant in the gas phase chemistry of the lower atmosphere. It efficiently controls atmospheric levels of methane (a major greenhouse gas), carbon monoxide, compounds of sulfur, nitrogen, and a number of other compounds such as hydrocarbons. This central role of OH as a gas phase "detergent" defines to a large part the self-cleansing power or the so-called "oxidation capacity" of the atmosphere [1]. The dominant primary source for OH in the lower troposphere is photolysis of ozone at wavelengths below 320 nm:

$$O_3 + h\nu \rightarrow O(^1D) + O_2 \quad (1)$$

$$O(^1D) + H_2O \rightarrow 2\ OH \quad (2)$$

Typically, 10% of the $O(^1D)$ reacts with water vapor according to Eq. (2) (assuming a H_2O mixing ratio of 1%). Most of the $O(^1D)$ is energetically quenched to

* Corresponding author. E-mail: harald.berresheim@dwd.de

[1] Also affiliated with the Georgia Institute of Technology, Atlanta, GA.

[2] Present address: Georgia Institute of Technology, Atlanta, GA.

PII S1387-3806(00)00233-5

the ground state, $O(^3P)$, by collision with O_2 or N_2. OH has an average lifetime of a few seconds or less and maximum concentrations of only 10^6–10^7 molecules cm^{-3} (or 0.04–0.4 parts per trillion by volume, pptv) in the lower troposphere. Therefore, measuring OH in ambient air presents a major experimental challenge.

Gaseous sulfuric acid, H_2SO_4, is mainly produced from the oxidation of SO_2 by OH:

$$SO_2 + OH + M \rightarrow HSO_3 + M \quad (3)$$

$$HSO_3 + O_2 \rightarrow SO_3 + HO_2 \quad (4)$$

$$SO_3 + H_2O + M \rightarrow H_2SO_4 + M \quad (5)$$

In the atmosphere H_2SO_4 is predominantly removed by deposition to aerosol particles and by absorption into droplets. The atmospheric lifetime of H_2SO_4 in the gas phase varies between a few minutes and about 1–2 hours. Similar to OH, atmospheric H_2SO_4 concentrations show a strong diurnal variation, typically from as low as 10^4 molecules cm^{-3} at night to daytime maxima in the 10^6–10^7 molecules cm^{-3} range. Because H_2SO_4 has a very low vapor pressure under atmospheric conditions (below 10^{-4} Pa) [2–4] special attention has been given in recent years to its role in gas-to-particle conversion, a process that includes homogeneous condensation of H_2SO_4, possibly in combination with other neutral compounds or atmospheric ions, forming molecular clusters that may subsequently grow to stable submicrometer size particles [e.g., 5–7]. Once these particles have reached a few hundred nanometers in diameter they efficiently scatter sunlight and play a crucial role in the formation of clouds and the regulation of global climate. There is a strong need for reliable measurements of H_2SO_4 to better understand these important processes and their potential modification by man-made sulfur emissions [8].

Both OH and H_2SO_4 have for a long time eluded detection and measurement in the atmosphere. Using CIMS-based techniques, H_2SO_4 was for the first time measured in the stratosphere by Arnold and Fabian [9], and in the troposphere by Eisele and Tanner [10]. Previous attempts to measure atmospheric OH were only partially successful either because of relatively low sensitivities or measurement interferences associated with the corresponding techniques [11–13]. Only in recent years after substantial improvements and with the development of several new techniques have atmospheric OH measurements become more successful [e.g., 14–18]. Among these new developments one of the most sensitive and versatile methods is atmospheric pressure chemical ionization mass spectrometry (AP/CIMS).

In the present work we describe a new AP/CIMS system that has been specifically designed and tested for long-term stationary field measurements but which, in principle, can also be used on mobile platforms or in laboratory studies. The present AP/CIMS system is an outgrowth of previous MS-based techniques that have been successfully applied for measuring atmospheric positive and negative ions, sulfur compounds, hydrocarbons, and OH [10,19–25]. Major features distinguishing the present system from previous versions include the use of different vacuum pumps (cryopumps) and an improved OH calibration unit. However, what is even more distinguishing from previous work is the goal of applying the present system for long-term measurements. Therefore, an extensive evaluation of the present performance of the system and, in particular, of potential measurement interferences is given in this work based on preliminary experiences from two years of test runs and ambient air H_2SO_4 and OH measurements.

The present AP/CIMS system has been developed and installed at the Meteorological Observatory Hohenpeissenberg (MOHp), a mountain research station operated by the German Weather Service (DWD). The station is located approximately 50 km north of the Alps at an elevation of about 1000 m above sea level. There are no major industrial sources in the vicinity. The station is mainly surrounded by forests and agricultural pastures. As part of DWD's atmospheric chemistry and climate research program the system has been operated since April 1998 measuring both H_2SO_4 and OH concentrations in the ambient atmosphere (on 151 days in 1998 and 186 days in 1999). It has also been successfully operated on the

west coast of Ireland in June 1999 as part of the EU project PARFORCE (New Particle Formation and Fate in the Coastal Environment). The complete results of these measurements will be published separately in the near future.

2. Experimental

2.1. Measurement principles

The techniques used in the present study to measure atmospheric H_2SO_4 and OH both employ negative chemical ionization converting H_2SO_4 molecules into HSO_4^- core ions by reaction with NO_3^- core ions at atmospheric pressure [9,26,27]:

$$H_2SO_4 + NO_3^- \rightarrow HSO_4^- + HNO_3 \quad (6)$$

The majority of the NO_3^- reactant ions are clustered with neutral HNO_3 and/or H_2O molecules as $NO_3^-(HNO_3)_m(H_2O)_n$ ($m = 0$–2, $n = 0$–3). However, because all of these compounds have been shown to react with H_2SO_4 at similar rates ([26]; for a detailed discussion see also [20]) they will be addressed simply as NO_3^- in the following text. The NO_3^- reactant ions are generated by a radioactive alpha emitter (^{241}Am) in a sheath gas flow of purified air enriched with HNO_3 vapor and high purity propane. The ion source is located in a region that is spatially separate from the chemical ionization region. This configuration and the presence of propane in the sheath gas effectively prevent metastable and radical species formed near the radioactive source from being mixed into the sample flow and interfering with the measurements.

The resulting HSO_4^- product ions are measured along with the NO_3^- reactant ions by a quadrupole mass spectrometer. The atmospheric H_2SO_4 concentration can be determined from the ratio of the signal counts obtained for both compounds, the interaction time t between sample air and NO_3^- ions, and the rate constant k for reaction (6):

$$[H_2SO_4] = \frac{1}{kt} \ln\left(\frac{[NO_3^-] + [HSO_4^-]}{[NO_3^-]}\right) \quad (7)$$

Based on the flow velocities and electrical fields that are continuously monitored, the interaction time was crudely estimated to be 0.15 s (which is uncertain by about a factor of 2; see also [10]). During this time interval only about 1% of the NO_3^- ions react to form HSO_4^-. Thus, the reaction does not significantly change the H_2SO_4 and NO_3^- concentrations in the center flow and Eq. (7) can be approximated by

$$[H_2SO_4] \approx \frac{[HSO_4^-]}{[NO_3^-]kt} \approx \frac{\{HSO_4^-\}}{\{NO_3^-\}kt} \quad (8)$$

In Eq. (8) and in the following text braces are used to symbolize signal counts whereas square brackets denote concentrations. In principle, no absolute calibrations of $[H_2SO_4]$ or knowledge of $[HSO_4^-]$ and $[NO_3^-]$ concentrations are necessary because the measurements are based on relative signal counts, i.e. signal ratios, and a fixed calibration constant $1/kt$. However, in addition to t, the reaction rate constant k (≈collision rate constant) is only known with an uncertainty of about a factor of 2 [27]. Therefore, in practice, the measurements are frequently calibrated as described below. This also helps to compensate for possible errors in the measurements such as wall losses of H_2SO_4 in the system.

Atmospheric OH is measured indirectly by extending the H_2SO_4 analytical method. Prior to the chemical ionization step OH is titrated by SO_2, which is added as a reactant gas to the sample flow. The corresponding reaction sequence is the same as shown in Eqs. (4)–(6). This results in an OH equivalent concentration of H_2SO_4 in addition to the ambient air H_2SO_4:

$$[OH] \approx F \frac{\{HSO_4^-\}_{TS} - \{HSO_4^-\}_{BS}}{\{NO_3^-\}} = F \frac{\Delta\{HSO_4^-\}}{\{NO_3^-\}} \quad (9)$$

In Eq. (9), F represents the calibration factor, which ideally should be equal to $1/kt$, and the subscripts TS and BS denote "total signal" and "background signal," respectively. As previously shown by Eisele and Tanner [24], the sensitivity and

precision of the OH measurement is significantly improved using isotopically heavy $^{34}SO_2$ as the titration gas to form $H^{34}SO_4^-$ ions that are detected at *m/z* 99 in the negative ion spectrum. The atmospheric isotopes $H_2{}^{34}SO_4$ and $H_2{}^{32}S^{18}O^{16}O_3$ contribute only a small background signal to *m/z* 99, representing about 5% of the total atmospheric H_2SO_4 concentration. On the other hand, $^{34}SO_2$ is rather expensive. When atmospheric H_2SO_4 levels are relatively low and less variable, OH titration using $^{32}SO_2$ may still provide a satisfactory sensitivity and precision for ambient air OH measurements. In this case, the OH concentration is obtained from the difference between the total $H^{32}SO_4^-$ signal and the background signal resulting from about 95% of the atmospheric H_2SO_4 concentration. Both signals are measured at *m/z* 97. At Hohenpeissenberg, either $^{32}SO_2$ or $^{34}SO_2$ is used for long-term measurements of OH depending on air quality and the desired sensitivity and precision of the measurements.

Reaction (4) produces the hydroperoxy radical, HO_2, as an intermediate product. In addition, daytime HO_2 concentrations in ambient air are typically 1–2 orders of magnitude higher than OH concentrations. Depending on the concentration of atmospheric nitrogen oxide (NO), the following reaction may significantly recycle OH in the sample flow:

$$NO + HO_2 \rightarrow NO_2 + OH \quad (10)$$

To minimize a positive measurement artifact from this reaction excess propane is added downflow from the SO_2 injection port to scavenge recycled OH molecules before they can react with SO_2 in the system. On the other hand, potential negative interferences in measuring OH may arise from reactions involving atmospheric NO_2, CO, and hydrocarbons (HC):

$$NO_2 + OH + M \rightarrow HNO_3 + M \qquad (M = N_2, O_2) \quad (11)$$

$$CO, HC + OH \rightarrow \text{Products} \quad (12)$$

In the atmosphere the OH–HO_2 system (also called the HO_x system) is generally in a photostationary balance. However, when air enters the inlet tube of the chemical ionization mass spectrometry (CIMS) instrument, its illumination by ambient light progressively decreases to zero. Eventually, ozone photolysis [Eqs. (1) and (2)] in the sample air is shut off. Nevertheless, corresponding changes in the OH concentration are small and will be neglected for two reasons. First, the time for OH to adjust to the new conditions (typically 1 s) is much longer than the transport time to the titration region (about 160 ms), and second, in ambient air the recycling of OH from HO_2 dominates substantially (typically 80%) over its primary production from ozone photolysis. Measurement uncertainties due to reactions (10)–(12) can be estimated based on concurrent measurements of OH and the respective reactant concentrations in ambient air and subsequent model calculations, as shown in the last part of this article.

In the following section the measurement principles are further discussed in conjunction with the structural features of the present apparatus. A schematic overview of the present AP/CIMS system is shown in Fig. 1. Additional information on performance tests conducted with different AP/CIMS system configurations can be obtained from prior publications by Eisele and co-workers [19,20,24].

2.2. Sample inlet and chemical titration region

Ambient air is drawn into the system through a turbulence-reducing scoop attached to a 10-cm-diameter, 30-cm-long inlet tube. The average center-of-flow velocity inside the tube is 5.2 m s^{-1} (at standard temperature and pressure, STP) as determined by manual pitot measurements. From the center of the inlet flow 10 standard liters (sl) min^{-1} are sampled through a 1.9-cm-diameter stainless steel sample tube into the ionization region of the apparatus (equivalent sample flow velocity: 0.59 m s^{-1}). The excess flow is vented back into the atmosphere. Flow conditions in the sample tube are quite laminar ($Re < 1000$). The sample flow is maintained by a constant mass flow difference induced in the ionization region (see next section). In previous configurations [19] a nozzle at the entrance of the sample tube has been used to make the sample inlet flow less susceptible to ambient wind turbulence. However, it was also reported that mea-

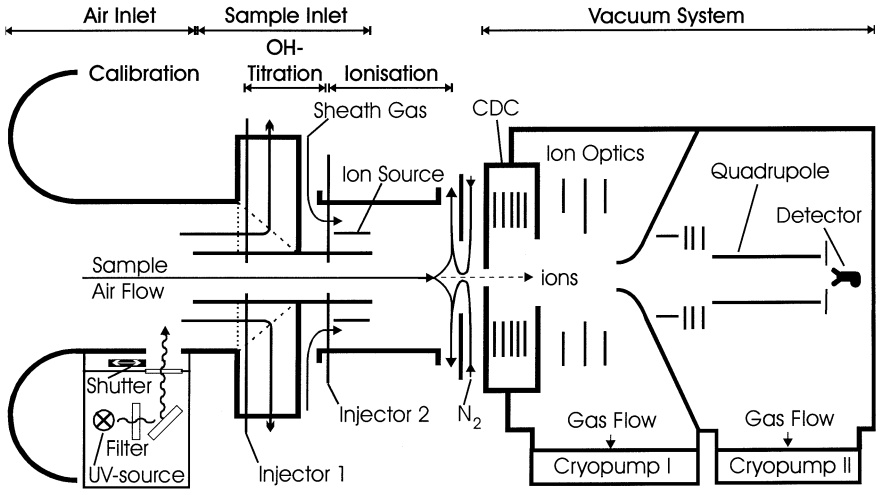

Fig. 1. Schematic overview (not scaled) of the major components of the Hohenpeissenberg AP/CIMS system including the calibration unit. Gas flows are indicated by solid arrows and the UV light path from the calibration source is shown as a wavy line. The overall dimensions of the system are: L 200 cm × W 100 cm × H 130 cm; total weight is approximately 300 kg. CDC = collision dissociation chamber.

surement sensitivity could be reduced by as much as 50% due to increased wall losses and turbulence downflow from the nozzle.

Inside the sample tube OH is chemically titrated according to Eqs. (3)–(5). Reactant and buffer gases (SO_2, N_2, C_3H_8) are introduced to this region through consecutive pairs of opposed stainless steel needle injectors intruding into the tube. Three pairs of injectors (denoted in flow direction as I, II, III in the following text) are installed in the present system. For simplicity, only two pairs are shown in Fig. 1. The first pair (I) is installed at a 32 mm distance from the sample tube inlet. The distances between the individual injector pairs are 16.3 mm (I–II), 36 mm (II–III), and 52.3 mm (I–III), respectively. In general, the latter injector configuration is used for the OH measurements at Hohenpeissenberg.

To perform an OH measurement, SO_2 is continuously mixed into the sample flow along with N_2 (ultra-high purity grade) through the first injector pair (I). Typically, SO_2 mixtures ranging between 0.5 and 2 vol.% are supplied to the system at flow rates between 20 and 5 sml min^{-1}, respectively. This produces an SO_2 mixing ratio of approximately 10 ppmv in the sample flow that completely titrates the OH within about 20 ms [19].

Before entering the sample tube SO_2 is premixed with N_2, with the N_2 flow being adjusted to give a total flow of 21 sml min^{-1}. A second flow (4.4 sml min^{-1}) is added to the mixture through a zero-dead space valve switching every 15 s between N_2 and 99.95 vol.% pure propane (C_3H_8). The addition of propane to the sample flow through the first injector pair produces a background signal [BS, see Eq. (9)] based on the reaction of propane with OH. The rate constant for this reaction is approximately equal to that of the SO_2 + OH reaction (1.1×10^{-12} cm^3 $molecules^{-1}$ s^{-1} and 0.85×10^{-12} cm^3 $molecules^{-1}$ s^{-1}, respectively, at 298 K [28]). Therefore, at typical SO_2 and propane mixing ratios in the sample flow of 10 ppmv and 400 ppmv, respectively, the OH reacts with propane about 40 times faster than with SO_2. Under these conditions more than 98% of the OH in the sample flow is consumed by propane. As mentioned in the previous section, a second flow of propane (4 sml min^{-1}) is added continuously through the rear set of injectors (III) to scavenge OH molecules produced from the reaction of HO_2 with NO in the sample air.

All reagents added to the system require a high degree of purity. Propane was purchased from two different manufacturers (MG Industries, AGA). Al-

though each cylinder filling was certified for the same purity grade of propane (99.95 vol%), a small negative offset in the OH measurements resulted sometimes from unknown trace impurities in individual cylinders. This is further discussed below in conjunction with Fig. 5. Either $^{32}SO_2$ or $^{34}SO_2$ is used for titrating OH. Both compounds can be supplied from commercial manufacturers. However, we prefer to prepare appropriate mixtures of either compound in our laboratory using elemental ultra-high purity ^{32}S (99.999%, C. Roth, Karlsruhe) or 90–99.8% enriched ^{34}S (EG&G Mound, Miamisburg; Cambridge Isotope Lab., Andover), respectively. The elemental sulfur is first dried and then burned in a clean 10 liter glass bulb containing an excess amount of ultra-high purity oxygen. The resulting SO_2 is separated from the remaining O_2 and transferred into a clean cryo-cooled gas cylinder and finally pressurized with N_2 to obtain the desired SO_2 mixing ratio in the cylinder (typically 1–2 vol.%). The amount of SO_2 required for complete titration of OH in the sample flow is experimentally determined by generating a known OH concentration (10^7–10^8 cm^{-3} range) and gradually increasing the SO_2 mixing ratio in the sample flow until a constant signal is obtained. Twice the corresponding SO_2 mass flow is then used for ambient air OH measurements.

2.3. Ionization region

As shown in Fig. 1, the sample tube protrudes into the ionization region where NO_3^- reactant ions are supplied from a sheath gas flow and focused into the center region by a concentrical electrical field to mix and react with the sample H_2SO_4 molecules. The sheath gas (ambient air purified by active charcoal and silica gel to remove particles, SO_2, and other trace gases) enters the ion source region through laminar flow stainless steel screens, typically at 46 sl min^{-1}. Just before the ion source region, propane is added continuously to the sheath gas at 10 sml min^{-1} to remove OH radicals produced by the source. Also near this point, HNO_3 vapor is continuously added to the sheath gas by a 5 sml min^{-1} N_2 carrier gas flow passing through the head space of a Peltier-cooled reservoir of concentrated liquid HNO_3 (held at about 12 °C). The NO_3^- reactant ions are produced by α bombardment from a radioactive ^{241}Am-source that is concentrically attached to a separate tube in the center of the sheath gas flow. Although the resulting negative ion spectrum is dominated by NO_3^- and clusters containing NO_3^-, a significant fraction of other ions such as CO_3^- are also produced (comparable to the relative formation of negative ions in the lower atmosphere [29]). Therefore, the sheath gas is enriched with HNO_3 to minimize the presence of these other ions. The total exhaust flow from the ionization region is typically 56 sl min^{-1}. Thus, the difference between sheath and exhaust flow maintains the 10 sl min^{-1} sample flow into the region. The exhaust flow is filtered through active charcoal cartridges and vented back into the atmosphere at a minimum distance of 50 m from the sampling point. From the ion cloud forming around the sample flow axis both reagent and product ions are forced by an electrical field (approximately 50 V cm^{-1}) to enter the vacuum region through a 200 μm diameter aperture ("pinhole"). A small 1 sl min^{-1} counterflow of dry N_2 gas on the atmospheric pressure side of the pinhole helps to prevent air molecules from entering the vacuum region, in particular H_2O molecules that may otherwise form higher order clusters upon adiabatic expansion and cooling.

2.4. Vacuum analysis region

The vacuum housing of the Hohenpeissenberg AP/CIMS system was designed to be as compact as possible with minimum pumping volume. In principle, the whole system can be operated in different positions (horizontal, vertical), and on mobile platforms such as ships or aircraft. The housing was custom-built including optional flanges for vacuum pumps, electronic feedthroughs, and a 0.2 mm maximum tolerance for both plane parallelity and paraxiality between the different components inside the vacuum system (Kurt Lesker Co., Hastings, England).

In flow direction, the vacuum region behind the pinhole begins with an entrance segment known as the "collision-dissociation chamber" (CDC). The pressure in the CDC is typically in the 10^{-1} hPa range.

Most of the ions entering the CDC are clustered with neutral ligand molecules such as HNO_3. In the CDC these ligands are removed from the core ions by low energy collisions of the clusters with N_2 molecules. The mean collisional energy is controlled by an accelerating positive electrical field ($E = 10$ V cm^{-1}) between the entrance and the exit of the CDC.

From the CDC the declustered core ions enter the first high vacuum chamber through a 1.5-cm-diameter aperture. The pressure in this region is approximately 2×10^{-3} hPa. Here the ions are refocused by an array of electronic lenses and submitted to the second high vacuum chamber (pressure approximately $2–3 \times 10^{-5}$ hPa) through a skimmer. The second chamber contains another set of focusing lenses—the quadrupole mass-filter (3/4 in. rods; Extrel) and the electron multiplier detector ("channeltron," 1 in. orifice; De-Tech) with associated signal amplifier electronics.

The high vacuum region is differentially pumped by two cryogenic pumps (Ebara models ICP300 and ICP200; N_2 pumping speeds: 3000 l s^{-1} and 1500 l s^{-1}, respectively) operating with liquid helium. Both pumps are flanged to the vacuum housing through electropneumatic gate valves that can be controlled either manually or automatically through electronic safety circuits. Each pump produces a high vacuum by freezing out gas molecules on two sequential cooling stages. Operating temperatures are approximately 60–80 K on the first stage and 10–20 K on the second stage. Typically, the pumps are heated out after about 14 days of continuous operation. The associated software-controlled regeneration cycle requires only about 5 h. Within another hour the vacuum housing is reevacuated and the system is again ready for operation.

2.5. Calibration

Both H_2SO_4 and OH measurements are calibrated based on known OH concentrations generated in the sample air. Ambient water vapor is photolyzed in the air inlet tube by a UV light source yielding an equal number of OH molecules and H atoms, the latter being rapidly converted to an equivalent number of HO_2 molecules by reaction with O_2. Concurrently, the H_2O concentration is determined using a capacitive humidity sensor or, more recently, a high-precision chilled mirror dewpoint hygrometer (Michell Instruments, model S4000). The main components of the calibration unit are indicated in Fig. 1. The photolyzing radiation centered at $\lambda = 184.9$ nm is produced by a Pen Ray mercury lamp that is thermally stabilized at 43 °C to provide a constant photon flux. The Pen Ray light beam is guided through an optical filter, reflected by an aluminum mirror, and passed through a rectangular suprasil quartz window into the air inlet tube. The optical filter transmits a narrow 22 nm band around the 184.9 nm line (peak transmission: 16%), thus eliminating potential interferences from the photolysis of ozone at $\lambda = 254$ nm. All major components (lamp, filter, mirror, window) are installed in a compact housing and continuously purged with nitrogen. The beam exit slit in the inlet tube wall is opened and closed by an automatic shutter.

Calibrations are performed both manually ("mappings") and automatically ("calibration checks" or "calchecks"). In each manual calibration the number of absorbed photons that generate OH radicals in a unit volume of the sample gas is determined. The incident UV photon flux (photons per unit area and time) is scanned in flow direction over the entire illuminated region upflow from the sample inlet tube. Photon flux values are calculated from the product of the current, i_{map}, measured per unit area using a solar-blind CsI photocathode (Hamamatsu model R5764) in conjunction with a Keithley model 614 picoampere meter, and the sensitivity D of the cathode at $\lambda = 184.9$ nm. Two different cathodes are currently used in turn. The spectral sensitivities of the cathodes (given in [W/mA] or [photons/As]) are known from certified measurements by the Physikalisch-Technische Bundesanstalt (PTB, Berlin, Germany). The cathode used for calibration is mounted on a precision two-axis positioning system and has an aperture of 4 mm × 4 mm. By summing up the scanning measurements made in adjacent 4 mm intervals along the flow axis and averaging the resulting integrals over an effective sample flow diameter (7 mm, calculated from the flow velocity profile) a "linear" total photon flux P is obtained (photons per

time and unit length in perpendicular direction to both the flow axis and the incident light beam. The generated OH concentration produced from the photolysis of ambient H_2O can then be calculated by Beer's law using P in conjunction with a unit length L (= 1 cm in the direction of the incident light beam), the flow velocity v in front of the sample inlet, the measured water vapor concentration $[H_2O]$, and the absorption cross section σ of water vapor at 184.9 nm (7.14×10^{-20} cm^2 at 25 °C; [30]):

$$[OH]_{UV,calc} = (P/vL)[1 - \exp(-\sigma[H_2O]L)] \quad (13)$$

Subsequently, a "mapping" value F_{map} is derived by relating the theoretically determined concentration $[OH]_{UV,calc}$ to the corresponding measured signal counts:

$$F_{map} = [OH]_{UV,calc} \frac{\{NO_3^-\}}{\{HSO_4^-\}_{TS} - \{HSO_4^-\}_{BS}} \quad (14)$$

In this case $\{HSO_4^-\}_{TS}$ represents the total signal corresponding to the sum of UV-generated OH, ambient air OH, and ambient air H_2SO_4 concentrations, whereas $\{HSO_4^-\}_{BS}$ is the total signal produced by only the ambient air concentrations of OH and H_2SO_4.

Mappings are typically repeated once every 1–2 months for the long-term measurements at Hohenpeissenberg. From averaging several F_{map} values obtained over a longer-term period of, say, 6–12 months, a single calibration factor F [Eq. (9)] is derived and used as a representative value for the same total period. Because H_2SO_4 and OH are both measured based on the corresponding yields of HSO_4^- product ions [Eq. (6)], the same calibration factor is used to determine both $[H_2SO_4]$ and [OH] concentrations in ambient air [in combination with Eqs. (8) and (9), respectively].

Calibration checks are typically conducted every 30 min between measurements to monitor short-term variations of the instrument's sensitivity. They consist of opening the shutter for about 5 min and measuring [OH] versus $[H_2O]$ concentrations. This yields, in each case, a "calcheck" value F_{check}:

$$F_{check} = \frac{[OH]_{UV,calc}}{[OH]_{UV,meas}} F \quad (15)$$

Here, $[OH]_{UV,meas}$ represents the measured UV-generated OH concentration that is derived according to Eq. (9).

Variations of F_{check} (and F_{map}) may be induced by interferences from ambient parameters, e.g. high NO, NO_2, or CO concentrations, or process parameters, e.g. instabilities in flow velocities or in P. In order to check the stability of the instrument's performance, a number of process parameters are continuously monitored, e.g. the flow velocity near the inlet wall that is measured by a built-in pitot tube. Also, the variability of P can be monitored by installing a cathode at the inlet wall across from the shutter slit.

3. Results and discussion

3.1. Measurements, tests, and improvements

Over the past two years our CIMS instrument has mainly been operated in the negative ion mode, although occasionally we have also recorded spectra of positive ions resulting from H_3O^+ proton transfer to sample air molecules. In general, a much higher number of masses with significant ion signals are observed in the positive ion mode. When operating in the negative ion mode sufficient HNO_3 vapor is added to the ion source region to produce almost exclusively NO_3^- reactant ions, primarily as $NO_3^-(HNO_3)$. Other negative ions such as O_2^- or CO_3^- rapidly transfer their charges to HNO_3 (typically within milliseconds) because the NO_3 group possesses a much higher electron affinity or acidity. Because there are only very few compounds in ambient air with acidities higher than HNO_3 [predominantly H_2SO_4 and—in the marine atmosphere—methanesulfonic acid ($CH_3S(O_2)OH$) that is detected at *m/z* 95] a relatively "clean" negative ion spectrum (showing only a few significant mass signals) is usually measured. An example for a spectrum obtained in the marine atmosphere is shown in Fig. 2. Except for the mass peaks recorded at *m/z* 95 and *m/z* 175 this is also typical for

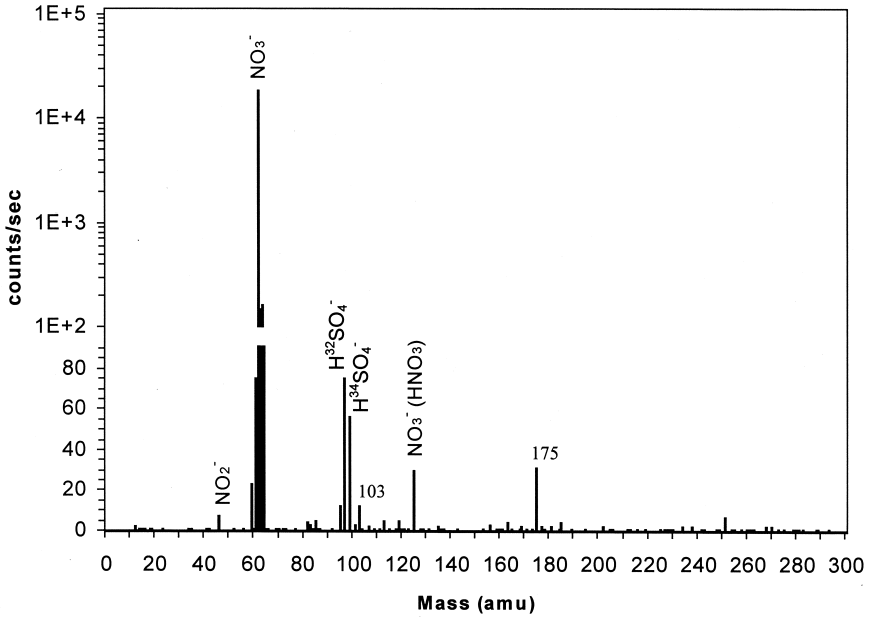

Fig. 2. Negative ion spectrum obtained from measurements of H_2SO_4 and OH concentrations using $^{34}SO_2$ to titrate OH (collision chamber voltage: −54 V). The spectrum was recorded in the clean marine atmosphere but is also typical for ambient air conditions at Hohenpeissenberg, except for mass peaks at *m/z* 95 (methane sulfonic acid) and *m/z* 175 (unidentified). The mass peak at *m/z* 103 is tentatively ascribed to malonic acid. Mass resolution is deliberately broadened (±0.5 amu half width) to minimize signal interferences from minor mass shifts. Contributions to mass signals at *m/z* 61, 63, and 64 partially arise from this broadening and from isotopes of O and N. Note that a linear scale is used on the bottom to show signal and background ion count rates, and a log scale is used to show the large dynamic range between reactant and product ion concentrations.

the spectra observed at Hohenpeissenberg. In general, the sensitivities obtained for the major signals at *m/z* 62, 97, and 99 are in very good agreement with previously published CIMS spectra for similar operating and ambient air conditions (e.g. Fig. 2(a) in [19]).

However, occasionally additional compounds were detected in the negative spectrum that significantly interfered with the OH and H_2SO_4 measurements. For example, pronounced peaks at *m/z* 69, 113, and 176 were observed when PFA teflon tubing (instead of stainless steel tubing) was used in the N_2 carrier gas line. Fig. 3 shows observations made on a hot summer day, when the N_2 line was partially exposed to direct sunlight. Clearly, the NO_3^- signal at *m/z* 62 was anticorrelated with the *m/z* 113 signal, which itself showed a strong positive correlation with temperature and sunlight intensity. Corresponding integral mass spectra showed that a number of compounds with masses larger than *m/z* 200 (not resolved) were also present in the system. The compound measured at *m/z* 113 was tentatively identified (by tandem mass spectrometric analysis at NCAR, Boulder) as trifluoroacetic acid minus a proton (CF_3COO^-; TFA^-). It is slightly more acidic than HNO_3. The mass signal observed at *m/z* 176 corresponds to the adduct compound $TFA^-(HNO_3)$. Consistent with these results, further fragmentation by tuning the CDC voltage to −100 V resulted in a decrease of the mass signals at *m/z* 69 (CF_3^-) and *m/z* 113 and a significant increase of the F^- signal at *m/z* 19. This example demonstrates the importance of spectral analyses for identifying potential measurement interferences. Therefore, negative ion spectra are frequently recorded between our long-term OH and H_2SO_4 measurements.

In the atmosphere, both OH and H_2SO_4 concentrations show significant diurnal variations consistent with the respective photochemical production and

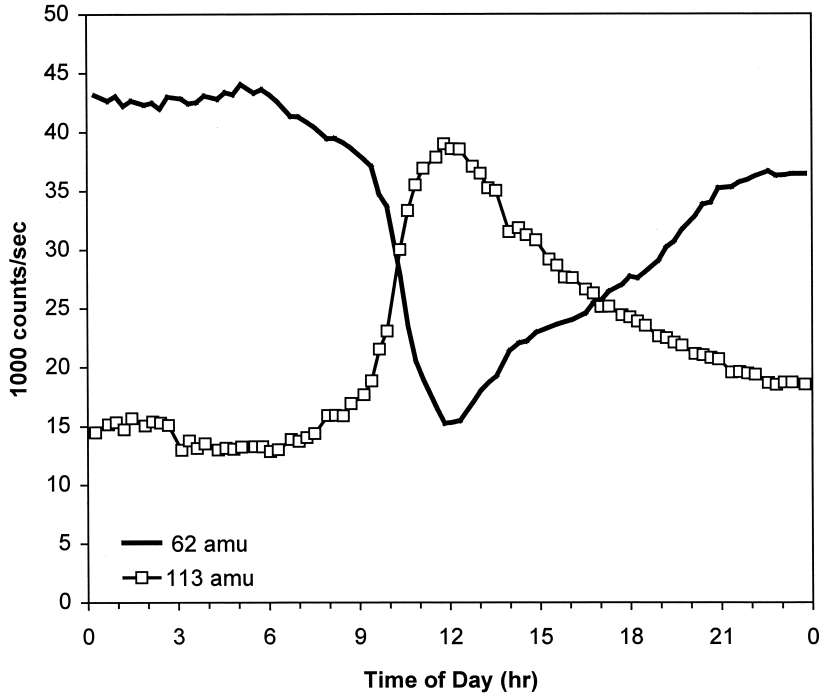

Fig. 3. Time series of a negative interference in the NO_3^- signal (*m/z* 62) observed on May 9, 1998. This interference was caused by elevated concentrations of a compound identified as trifluoroacetate (TFA^-, *m/z* 113). The source of this compound was teflon tubing which, on this day, was used in the N_2 supply line of the CIMS system. The tubing was exposed to ambient sunlight and temperature yielding a maximum TFA^- interference signal around midday.

specific removal processes of both compounds. Typical examples of diurnal variations of [H_2SO_4] and [OH] measured at Hohenpeissenberg are shown in Fig. 4(a) and (b). Measurements were made with a 30 s time resolution and alternated between H_2SO_4, OH, and calcheck modes every 10 min, respectively. The diurnal patterns and concentration ranges of H_2SO_4 and OH observed at Hohenpeissenberg may be considered typical for background continental boundary layer air in northern midlatitudes. They are comparable to previous measurements made by other investigators at different sites in the continental United States and in Germany. H_2SO_4 concentrations measured in spring and summer ranged from 1×10^5 cm^{-3} (night) to $>10^7$ cm^{-3} (midday) [10], and OH concentrations ranged from $<10^5$ cm^{-3} (night) to midday maxima around $6–8 \times 10^6$ cm^{-3} in fall [19] and $7–14 \times 10^6$ cm^{-3} in summer [14–17,31]. The present study is the first to report wintertime H_2SO_4 and OH measurements in the midlatitudinal continental atmosphere [Figs. 4(a) and (b)]. Similar to previous observations by Eisele and Tanner [10] our measurements frequently (in all seasons) showed the presence of significant nighttime H_2SO_4 concentrations in the upper 10^5 cm^{-3} range (occasionally up to 2×10^6 cm^{-3}) even in relatively clean air [Figs. 4(a) and (b)]. A preliminary evaluation of the total data set accumulated until now suggests the existence of an unknown atmospheric source contributing to these nighttime (and possibly also to daytime) H_2SO_4 levels.

A comparison between the 30 s time-resolved OH data shown for December 26 and 29, 1998, demonstrates the significant improvement in OH measurement precision that could be achieved by changing the titration gas from $^{32}SO_2$ to $^{34}SO_2$. Since the end of 1998 $^{34}SO_2$ has consistently been used for high-precision daytime OH measurements with a much lower OH background signal at *m/z* 99 compared to

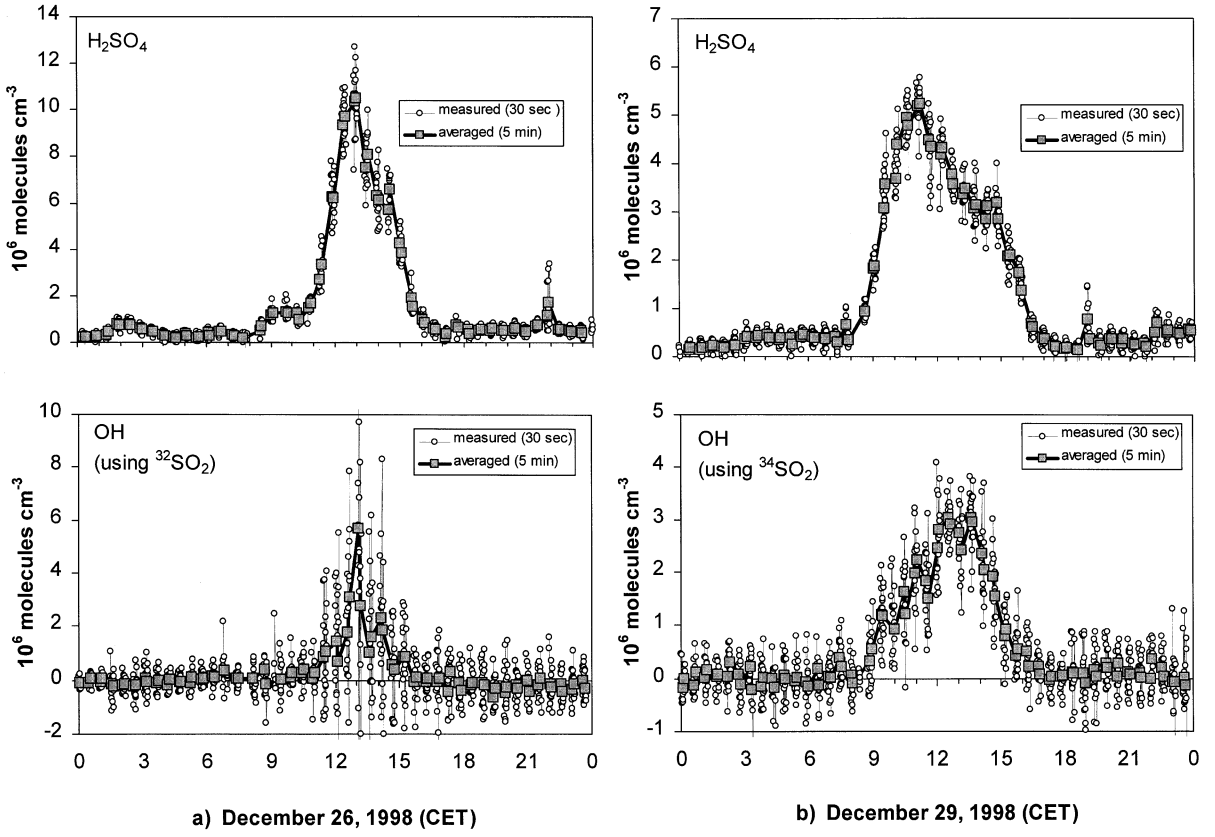

Fig. 4. Typical diurnal variations of atmospheric H_2SO_4 and OH concentrations measured with 30 s time resolution in 10 min intervals (circles). The results for each 10 min interval are also shown as two 5-min average values (squares). Results from two different days are presented, demonstrating the significant improvement in OH measurement precision from using (b) $^{34}SO_2$ instead of (a) $^{32}SO_2$ as titrant gas (with similar ambient H_2SO_4 concentrations).

the *m/z* 97 H_2SO_4 signal. Another possibility of testing the quality of our present OH measurements is by comparing the results with independently measured values of $j(O^1D)$, the ozone photolysis frequency corresponding to reaction (1) that is measured by filter radiometry (1 min resolution). Fig. 5 shows an example demonstrating a very good correlation ($r = 0.96$) between corresponding diurnal cycles measured for both parameters on September 4, 1999. Slightly negative OH values were obtained after 18:00 CET. As mentioned earlier, we are aware that a negative offset may sometimes be produced from interferences by trace impurities in the propane reagent gas that could react with the SO_2 in the system and produce an elevated background signal. However, the example in Fig. 5 shows no similar offset for the early morning of the same day. Other possible explanations for such negative interferences will be explored in future tests.

3.2. Error analysis and detection limits

As presented in Sec. 2, the concentrations of H_2SO_4 and OH are calculated according to Eqs. (8) and (9), respectively. Thus, uncertainties in the measurements can be estimated in a first approach by error propagation of the involved quantities. In the following text the results of this analysis will be referred to as "instrumental uncertainties." In addition, the measurements can also be influenced by changes in ambient parameters, e.g. wind conditions or the chem-

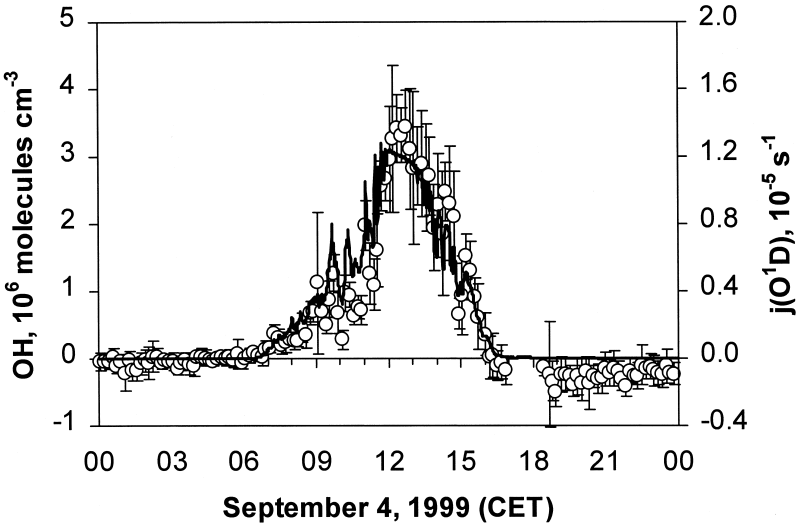

Fig. 5. Correlation between atmospheric OH concentrations (circles: 5-min averages, vertical bars: standard deviations) and the ozone photolysis frequency, $j(O^1D)$, measured on September 4, 1999.

ical composition of the air [Eqs. (10)–(12)]. Furthermore, these changes can differ in their relative impacts on calibration and ambient air measurements. Therefore, both instrumental and ambient parameters will be taken into account to estimate the total uncertainties of the calibration and ambient air measurements, respectively. Finally, for calibration measurements the calculated precisions will be compared with the observed reproducibility of the calibration measurements.

3.2.1. Calibration

Instrumental uncertainties during calibration can be directly estimated from Gaussian error propagation calculations based on Eqs. (13)–(15). Our present uncertainty estimates for the various parameters are summarized in Table 1. Separate values for precision and accuracy are given for each parameter. Precision estimates were based on estimated uncertainties or observed variations resulting from nonreproducible effects, whereas accuracy estimates represent overall uncertainties that also include systematic errors.

The flow velocity v was measured independently with both a pitot tube and a hot wire anemometer. Errors in v were calculated from corresponding uncertainties in both methods and the relative differences in the obtained results. The uncertainty of the

Table 1
Estimated uncertainties (2σ) of the Hohenpeissenberg CIMS system for OH and H_2SO_4 calibration and ambient air-measurements. Typical count rates are given as "cts in s" (counts in seconds); chemical impact estimates are taken from Table 2

	Precision (%)	Accuracy (%)
Calibration		
$\{NO_3^-\}$ (55000 cts in 2 s)	2	2
$\Delta\{HSO_4^-\}$ (3000 cts in 8 s)	12	12
v	8	10
σ		3
$[H_2O]$	6	10
i(map)	4	6
D	9	20
Chemical impact (95 percentile)	39	39
Wind effect	30	30
F_{check}	53	57
F (total uncertainty, 5 mappings)	15	25
Ambient OH measurements		
$\Delta\{H^{34}SO_4^-\}$ (480 cts in 8 s)	46	46
$\Delta\{H^{32}SO_4^-\}$ (440 cts in 8 s)	72	72
Chemical impact (95 percentile)	35	35
[OH] using $^{34}SO_2$ (5 min average)	48	54
[OH] using $^{32}SO_2$ (5 min average)	51	57
Ambient H_2SO_4 measurements		
$\{H_2SO_4\}$ (500 cts in 8 s)	18	18
$[H_2SO_4]$ (5 min average)	30	39

absorption cross section σ of water vapor at 184.9 nm was given by Cantrell et al. [30] as 3% (Table 1). Measurements of the water vapor concentrations were performed in various time periods by different instruments (capacitive sensor, psychrometer, and, more recently, by a chilled mirror dewpoint hygrometer) with their respective accuracies and with uncertainties resulting from different sampling setups of the instruments. For most of the period evaluated in the present work an average dewpoint measurement accuracy of ± 1 °C was estimated corresponding to less than 10% uncertainty with respect to the observed changes in ambient air dewpoint (Table 1). An even lower uncertainty than reported in Table 1 is presently achieved by using a capacitive sensor for routine measurements and the chilled mirror dewpoint instrument for frequent calibrations. Both instruments are installed within about 1 m distance from the CIMS inlet. This setup results in a dewpoint uncertainty of less than 0.4 °C.

As mentioned earlier, the photon flux P was measured using two or three calibrated photocathodes and a picoamperemeter. Three calibrations of the photocathodes were performed in intervals of eight months by the PTB (Berlin, Germany). Corresponding D values (sensitivities) determined for each cathode partially increased between consecutive calibrations by up to 20%. Relative changes between the sensitivities of the three cathodes were less than 12% (2σ) over the whole period. These estimates are based on results obtained from both the cathode calibrations and the multicathode OH calibration measurements. The resulting precision of individual cathodes is thus estimated to be 9%, and the accuracy of the cathode measurements is 20%. Because the 9% precision already includes uncertainties due to cathode sensitivity, measurements of the current, i_{map}, and positioning of the cathode, this value is also valid for the measurement precision of the photon flux P. In "calcheck" measurements changes in ambient water vapor concentrations between the light source and the center flow produce an additional error in the measurement of P that is, however, on the order of only 2% for typical ambient conditions and can thus be neglected. In summary, if only instrumental uncertainties are considered, the 2σ precision of the calibration is estimated to be 19% and the accuracy 28% (not listed in Table 1).

In the following text we will also consider additional interferences in calibration measurements caused by ambient parameters (e.g. wind turbulence, reactive chemical species) that may occasionally produce significant errors. During calibration typically 5×10^7 molecules cm^{-3} of both OH and HO_2 are produced in the photolysis region. These levels are considerably higher than ambient OH concentrations. Consequently, the HO_x system is far off from stationary state conditions and relaxes back toward stationary state within characteristic times that depend on ambient trace gas concentrations, mainly of NO, NO_2, CO, and hydrocarbons [Eqs. (10)–(12)]. Characteristic times for readjustment to stationary state conditions are about 1 s for OH and 1 min for HO_2. The impact of nonstationary state conditions on calibration measurements can be rather complex because enhanced levels of NO_2, CO, and hydrocarbons (in particular isoprene) tend to reduce OH concentrations in the sample flow between the photolysis and first injector zones. At a flow velocity of 0.6 m s^{-1} this section provides a maximum available reaction time of 84 ms. In contrast, NO tends to increase the measured OH signal due to reaction (10) between the photolysis and rear injector zones (173 ms). Both negative and positive chemical interferences were calculated using a similar approach to that of Tanner et al. [19]. Corresponding changes in HO_x and H_2SO_4 concentrations in the sample inlet and titration regions of the CIMS instrument are shown in Fig. 6 for selected combinations of pertinent trace gas concentrations. In addition, calculated errors for OH calibration measurements ($[\mathrm{OH}]_{\mathrm{UV,meas}}$) with respect to changes in ambient concentrations of selected trace gases are given in Table 2. These estimates are based on daytime measurements and typical trace gas concentrations at Hohenpeissenberg also shown in Table 2; nighttime conditions would result in slightly higher error estimates.

The results suggest that ambient trace gas concentrations can have a significant impact on the OH calibration signal and the resulting calibration factor.

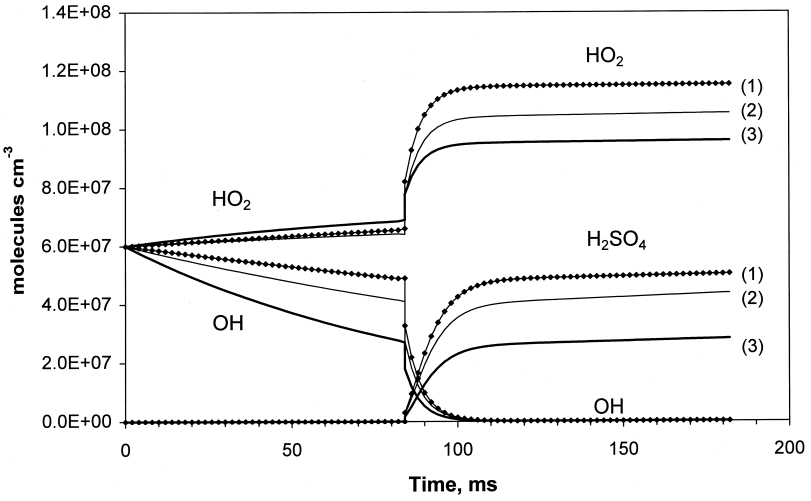

Fig. 6. Model simulations of the influence of different concentrations of NO, NO_2, CO, and hydrocarbons (HC) in ambient air on the calibration of OH and H_2SO_4. Assuming an initial UV-generated concentration of 6×10^7 molecules cm^{-3} for both OH and HO_2, the temporal profiles of the corresponding concentrations of OH, HO_2, and H_2SO_4 in the sample inlet are shown for the time elapsed since photolysis of the air sample (entrance of the sample inlet). Titration of OH is set to begin after 84 ms. Three different scenarios have been simulated: (1) NO = 0.2 ppb, NO_2 = 1 ppb, CO = 200 ppb, HC = 0.5/s, (2) NO = 2.0 ppb, NO_2 = 6 ppb, CO = 200 ppb, HC = 1.5/s, (3) NO = 2.0 ppb, NO_2 = 10 ppb, CO = 500 ppb, HC = 4.0/s. For HC a total OH reactivity value (sum of individual rate constants × HC concentrations), has been assumed for each scenario.

Relative to the theoretical value $[OH]_{UV,calc}$, the measured OH calibration signal is reduced for each case shown in Table 2, even for the base case assuming the relatively low median concentrations of NO, NO_2, CO, and isoprene (−13%). For the 5 percentile scenario, losses are reduced to 7%, how-

Table 2
Top section: Median, 5 percentile, and 95 percentile mixing ratios (in parts-per-billion by volume, ppbv) of NO, NO_2, and CO for the total period 1995–1998, and of daytime isoprene levels in June 1999, measured at Hohenpeissenberg. Middle and bottom sections: Calculated changes of OH concentrations (in %) between the sample inlet and ionization region as a result of chemical interferences from different trace gas mixing ratios. "Base case" assumes median mixing ratios and a turnover rate of 0.5 s^{-1} due to reaction of OH with hydrocarbons other than isoprene. Individual "5 percentile" and "95 percentile" estimates assume the respective value for the corresponding compound and median values for all other compounds. "Total" estimates are based on median, 5, and 95 percentile mixing ratios of all listed compounds, respectively (also, a hydrocarbon turnover rate of 2.5 s^{-1} was assumed in the "95 percentile" case); see text for further model assumptions

	NO	NO_2	CO	Isoprene	Total
Median	0.07	1.8	166	0.057	
5 percentile	0.03	0.45	95	0.001	
95 percentile	1.13	8.3	307	0.536	
Calibration: $[OH]_{UV,meas}$ deviation from $[OH]_{UV,calc}$ (%)					
Base case					−13
5 percentile	−13	−9	−10	−12	−7
95 percentile	−8	−25	−17	−19	−39
Ambient air measurements: $[OH]_{amb}$ deviation from true ambient [OH], (%)					
Base case					9
5 percentile	7	10	6	8	5
95 percentile	11	−2	14	16	35

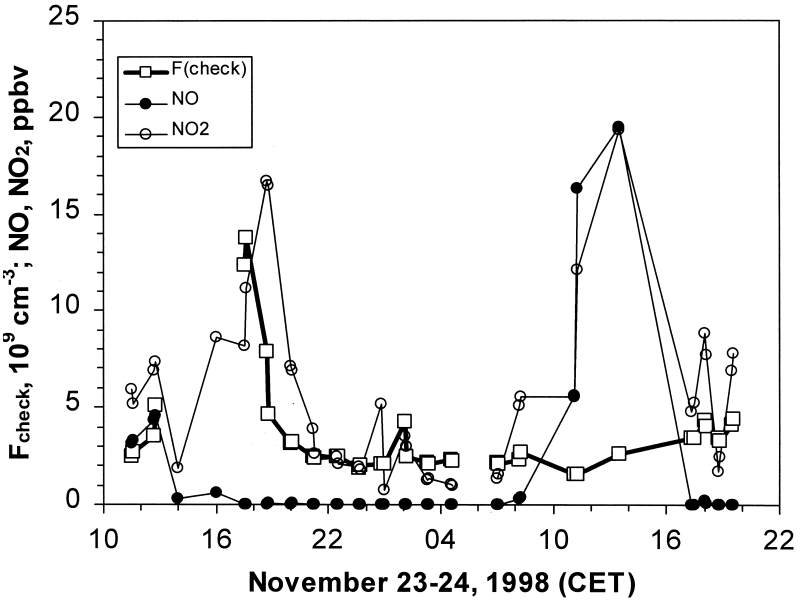

Fig. 7. Variations of the "calcheck" value, F_{check}, on two days with significant air pollution episodes as indicated by the corresponding NO and NO_2 mixing ratios (November 23–24, 1998). The ambient wind speed on both days was <3 m s^{-1}.

ever, the 95 percentile scenario causes measurement errors of 39%. Although both scenarios, which roughly bracket the 2σ ranges of the corresponding trace gas mixing ratios, are clearly unsymmetrical, we use 39% as a conservative estimate of the uncertainties due to chemical interferences estimated in Table 1. Fig. 7 shows an extreme example of "chemically induced" variations of F_{check} resulting from heavily polluted conditions on November 23–24, 1998, which, however, are rarely encountered at Hohenpeissenberg (see Table 2). Any measurement interferences by wind turbulence can be excluded because calm conditions prevailed on both days (wind speed <3 m s^{-1}). F_{check} values for "undisturbed" periods were in the range of 2–3 $\times$ 10^9 cm^{-3}. Clearly, the high values of F_{check} between 17:00 and 19:00 on November 23 [corresponding to low values of the measured OH calibration signal; Eq. (15)] were correlated with unusually enhanced NO_2 and CO mixing ratios (NO_2 up to 16 ppbv and CO up to 490 ppbv). In the same time intervals NO mixing ratios were mostly well below 1 ppbv. On the other hand, F_{check} values decreased slightly around 11:15 on November 24, when NO, NO_2, and CO mixing ratios increased to 16 ppbv, 12 ppbv, and 480 ppbv, respectively. Later, at 13:30, F_{check} returned to values typical for "undisturbed" conditions (2.7 $\times$ 10^9 cm^{-3}) although the air was heavily polluted by heating exhausts from nearby residences. However, at that time both NO and NO_2 mixing ratios were at the same level (19 ppbv each; CO: 650 ppbv) which resulted in a compensation of the corresponding opposite effects of NO and NO_2 on the OH calibration signal yielding a "normal" F_{check} value.

Fig. 8 shows a typical example for the influence of wind speed on the measured F_{check} values recorded on June 21, 1998. On this day the concentrations of all the trace gases considered in Fig. 6 and Table 2 were low enough to rule out any chemical interferences in measuring F_{check}. The observations suggest a positive correlation between F_{check} and wind velocity above approximately 5 m s^{-1}. Wind speed showed an impact on F_{check} values for horizontal as well as vertical air inlet configurations. Pitot measurements near the inlet wall close to the entrance of the sample tube showed an impact of ambient wind on the flow pattern in the air inlet region such that higher flow velocities were measured when wind blew across the

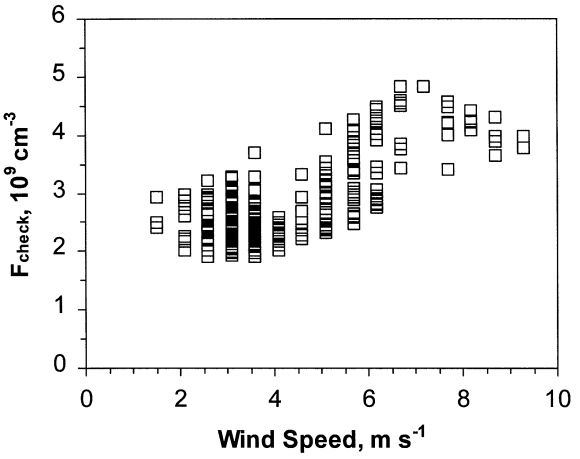

Fig. 8. Variations of the "calcheck" value, F_{check}, as a function of ambient wind speed (June 21, 1998). The air was relatively clean with ambient NO and NO_2 levels mostly around 1 ppbv each or lower.

inlet toward the side of the pitot tube (and vice versa). These effects may have enhanced flow turbulence and potentially induced losses of OH and H_2SO_4 in the sample tube and ion reaction region (wall losses and losses due to dilution of the sample flow with sheath gas). To estimate the potential error resulting from wind turbulence, the data in Fig. 8 were divided into nondisturbed (<5 m s^{-1}) and disturbed (>5 m s^{-1}) regimes. Corresponding average values for F_{check} were calculated as $(2.5 \pm 0.3) \times 10^9$ cm^{-3} and $(3.5 \pm 0.7) \times 10^9$ cm^{-3}, respectively, differing from each other by 42%. However, because wind velocity during measurement periods was mostly less than 5 m s^{-1} at Hohenpeissenberg, only a 30% uncertainty in F_{check} was attributed to "wind effect" in Table 1.

Combining the precisions of the instrumental and ambient parameters, a total precision for F_{check} of 53% is calculated. For comparison, an example for observed variations of F_{check} is shown in Fig. 9. From these data an average value of $(3.0 \pm 1.4) \times 10^9$ cm^{-3} and an overall precision of 46% were determined for F_{check} after excluding short-term episodes with fog conditions and/or significant air pollution (circled values in Fig. 9). Wind speed was always significantly less than 5 m s^{-1} in the corresponding period. Although estimated precision and observed variations of F_{check} appear to be comparable within a range of a factor of two, we cannot rule out the possibility of additional interferences by ambient parameters on F_{check} measurements that at this time have not yet been recognized or fully understood.

The observed reproducibility of F_{map} was determined from manual calibration measurements ("mappings") to be 34%. This figure is assumed to be only marginally influenced by ambient parameters because mappings were only performed on days with calm winds and low trace gas concentrations. This assumption is supported by the reasonable agreement between the reproducibility of F_{map} and the instrumental uncertainty in F of 19%. The total uncertainty of the calibration factor F (Table 1) is then calculated from the errors of the corresponding F_{map} values (data from 5 mappings have been used for the estimate in Table 1) and the systematic uncertainties in v, σ, $[H_2O]$, i(map), and D. A total precision of 15% and accuracy of 25% for F have been estimated in Table 1, with the UV cathode sensitivity D representing the largest individual error source in this estimate.

3.2.2. Ambient OH and H_2SO_4 Measurements

Uncertainties in ambient air OH concentration measurements are determined from the calibration factor F and the corresponding signal count rates [see Eqs. (9) and (14)]. Thus, error propagation has to consider F, count statistics, and potential wind and chemical interferences. Errors due to wind-induced turbulence are assumed to be similar to those in calibration measurements. Estimated sensitivities of ambient air OH measurements against changes in concentrations of selected trace gases are included in Table 2. For the corresponding calculations, a constant OH production rate from photolysis of O_3 of 2×10^6 cm^{-3} s^{-1} was assumed as well as stationary state conditions for the calculation of ambient air $[OH]_{amb}$ and $[HO_2]_{amb}$ resulting in OH concentrations of 4.0, 7.7, and 1.0×10^6 cm^{-3} for "base case," 5 percentile, and 95 percentile scenarios, respectively. This procedure was preferred to using prescribed $[OH]_{amb}$ because it accounts for the variations of $[OH]_{amb}$ under the various trace gas scenarios (see Table 2). It was found that chemical interferences

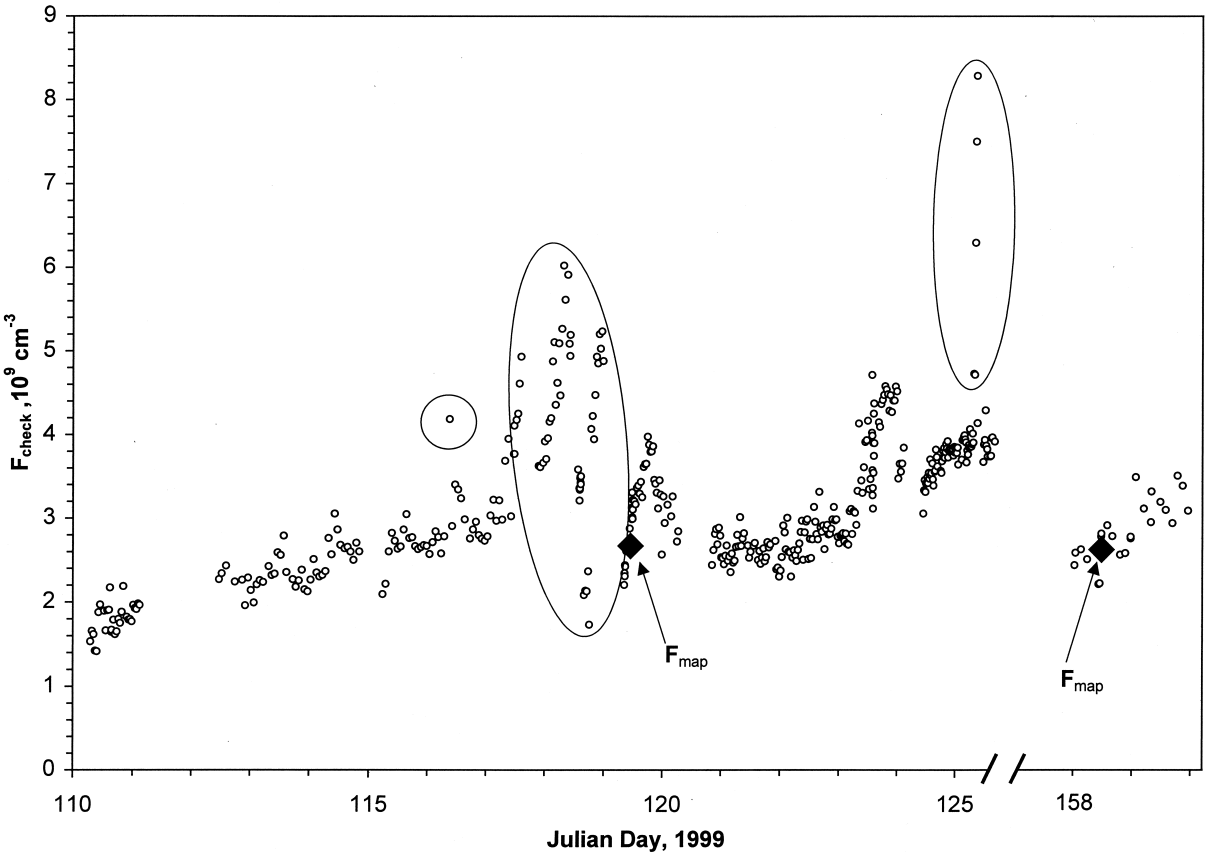

Fig. 9. Typical variations of the "calcheck" value, F_{check}, over a longer term period (April 20–May 5, and June 7–8, 1999). Also included are values for F_{map} determined in two corresponding manual calibrations ("mappings," see text). Circled data were correlated with significant interferences from instrumental and/or ambient parameters (see text) and have been excluded from statistical calculations. Using the remaining data an average F_{check} value of $(3.0 \pm 0.7) \times 10^9$ cm^{-3} was determined for the corresponding period.

could produce an overmeasurement of $[OH]_{amb}$ by as much as 5–35%. On the other hand, the same interferences could result in an undermeasurement of $[OH]_{UV,meas}$ levels during calibration runs. This different sensitivity results from the fact that only small deviations from stationary state occur in the "dark" inlet region during ambient OH measurements, in contrast to relatively large deviations during calibration measurements. In total, for OH measurements at 5 min time resolution using $^{34}SO_2$ as titration gas a precision of 48% and an accuracy of 54% is calculated from error propagation (Table 1). If $^{32}SO_2$ instead of $^{34}SO_2$ is used as titration gas, the numbers are slightly higher due to the higher background signal contribution by ambient H_2SO_4 concentrations. For very low OH concentrations the errors are determined by the detection limit (see below).

Errors in ambient air H_2SO_4 measurements (5 min time resolution) are smaller than for OH because they are measured without chemical titration and because H_2SO_4 has a relatively long lifetime in the ambient atmosphere (typically two or more orders of magnitude longer compared to OH). Thus, the corresponding precision is assumed to be determined only by wind effects and the reproducibility of the corresponding signal count rates. A value of 30% is estimated. The accuracy estimate for the H_2SO_4 measurements (39%) was derived by additionally accounting for the uncertainty in the calibration factor. For 30 s signal integration the

precision and accuracy estimates are 33% and 41%, respectively.

3.2.3. Detection limits

From the 2σ scatter of signal count rate measurements at nighttime, the corresponding detection limits for 5 min signal integration were calculated to be 2×10^5 molecules cm^{-3} for OH and 3×10^4 molecules cm^{-3} for H_2SO_4. However, for the present time we conservatively estimate the OH detection limit to be 5×10^5 molecules cm^{-3}. For most of the 2-yr measurement period considered here this value corresponds to the maximum negative offset signal observed at nighttime (see Fig. 5). The factors producing this variable offset signal are not yet fully understood and will be the subject of future studies.

4. Conclusions and future plans

We have described the present operating status of a new AP/CIMS system for long-term measurements of atmospheric OH and H_2SO_4 concentrations. A detailed error analysis has been conducted, including uncertainties from instrumental as well as ambient air parameters (wind and chemical interferences). With respect to H_2SO_4 measurements, CIMS methods originally developed by Eisele and Tanner [10] and by Arnold and co-workers [9,32] are unique in their sensitivity and time resolution. For our present system we estimate a H_2SO_4 detection limit of 3×10^4 molecules cm^{-3} based on 5 min signal integration; measurement accuracy and precision are 39% and 30%, respectively, for 5-min time-resolved measurements. With respect to atmospheric OH measurements, corresponding estimates are 5×10^5 molecules cm^{-3} for detection limit (5-min signal integration), 54% for accuracy, and 48% for precision (5-min time resolution). The largest contribution to the uncertainties in our present OH measurements is caused by variations in ambient parameters (wind and chemical interferences). Several aspects of the system performance under calibration and ambient air measurement conditions are not yet fully understood or can only be crudely quantified at this time. Therefore, our work in the near future—in addition to establishing a long-term record of ambient air H_2SO_4 and OH concentrations—will focus on continuously improving the performance of the system both by modifications of hardware components as well as optimization of operational parameters. For example, preliminary tests have shown that a reduction of the OH titration time by increasing the sample flow rate and/or reducing the distance between the front and rear injectors should yield a considerable improvement of the OH measurement precision and sensitivity. This may also require moving the front and rear injectors closer to the entrance of the sample inlet tube and using a nozzle to better stabilize the inlet flow against wind turbulence. Appropriate tests will be conducted with the overall goal to better quantify and minimize interferences by wind turbulence, chemical reactions in the presence of polluted air, drifts in instrumental parameters (optical and mass flow components), and surface wall losses in the system. In addition, field measurements are planned involving a side-by-side intercomparison with other OH-measuring systems such as Laser-induced fluorescence or differential optical absorption spectroscopy. Measurements in the positive ion mode will be another research objective in the future.

Acknowledgements

We would like to thank R. Weiner, P. Settele, and R. Ruf for helping with the installment of the CIMS system, improvements of the electronic components, contributions to various test and field measurements, and their assistance in data evaluation. We also thank S. Gilge for providing the NO, NO_2, and CO data. The technical development of the CIMS system and manufacturing or purchase of system components were entirely funded by DWD/BMVBW. Field measurements presented in this work were in part sponsored by DWD/BMVBW, the German BMBF Aerosol Research Program (AFS), grant 07AF201A/8, and by the European Commission through project PARFORCE, grant ENV4-CT97-0526.

References

[1] A.M. Thompson, Science 256 (1992) 1157.
[2] J.J. Marti, A. Jefferson, X.P. Cai, C. Richert, P.H. McMurry, F. Eisele, J. Geophys. Res. 102 (1997) 3725.
[3] R.J. Weber, J.J. Marti, P.H. McMurry, F.L. Eisele, D.J. Tanner, A. Jefferson, Chem. Eng. Commun. 151 (1996) 53.
[4] G.P. Ayers, R.W. Gillett, J.L. Gras, Geophys. Res. Lett. 7 (1980) 433.
[5] M. Kulmala, A. Laaksonen, L. Pirjola, J. Geophys. Res. 103 (1998) 8301.
[6] R.P. Turco, J.X. Zhao, F. Yu, Geophys. Res. Lett. 25 (1998) 635.
[7] R.J. Weber, J.J. Marti, P.H. McMurry, F.L. Eisele, D.J. Tanner, A. Jefferson, J. Geophys. Res. 102 (1997) 4375.
[8] IPCC, Climate Change 1995: The Science of Climate Change, J.T. Houghton, L.G.M. Filho, B.A. Callander, N. Narris, A. Kattenberg, K. Maskell (Eds.), Cambridge Univ. Press, Cambridge, 1996.
[9] F. Arnold, R. Fabian, Nature 283 (1980) 55.
[10] F.L. Eisele, D.J. Tanner, J. Geophys. Res. 98 (1993) 9001.
[11] U. Platt, M. Rateike, W. Junkermann, J. Rudolph, D.H. Ehhalt, J. Geophys. Res. 93 (1988) 5159.
[12] S.M. Beck, R.J. Bendura, D.S. McDougal, J.M. Hoell, G.L. Gregory, J.H. Curfman, D.D. Davis, J. Bradshaw, M.O. Rodgers, C.C. Wang, L.I. Davis, M.J. Campbell, A.L. Torres, M.A. Carroll, B.A. Ridley, G.W. Sachse, G.F. Hill, E.P. Condon, R.A. Rasmussen, J. Geophys. Res. 92 (1987) 1977.
[13] D. Perner, U. Platt, M. Trainer, G. Hübler, J. Drummond, W. Junkermann, J. Rudolph, B. Schubert, A. Volz, D.H. Ehhalt, K.J. Rumpel, G. Helas, J. Atmos. Chem. 5 (1987) 185.
[14] H.-P. Dorn, U. Brandenburger, T. Brauers, M. Hausmann, D.H. Ehhalt, Geophys. Res. Lett. 23 (1996) 2537.
[15] A. Hofzumahaus, U. Aschmutat, M. Hessling, F. Holland, D.H. Ehhalt, Geophys. Res. Lett. 23 (1996) 2541.
[16] T. Brauers, U. Aschmutat, U. Brandenburger, H.-P. Dorn, M. Hausmann, M. Hessling, A. Hofzumahaus, F. Holland, C. Plass-Dülmer, D.H. Ehhalt, Geophys. Res. Lett. 23 (1996) 2545.
[17] D.R. Crosley (Ed.), J. Atmos. Sci. (special issue) 52(19) (1995).
[18] D.R. Crosley (Ed.), Local Measurement of Tropospheric HO_x, Workshop report MP 92-135R, SRI International, Menlo Park, 1993.
[19] D.J. Tanner, A. Jefferson, F.L. Eisele, J. Geophys. Res. 102 (1997) 6415.
[20] D.J. Tanner, F.L. Eisele, J. Geophys. Res. 100 (1995) 2883.
[21] H. Berresheim, D.J. Tanner, F.L. Eisele, Anal. Chem. 65 (1993) 84.
[22] H. Berresheim, F.L. Eisele, D.J. Tanner, Anal. Chem. 65 (1993) 3168.
[23] F.L. Eisele, H. Berresheim, Anal. Chem. 64 (1992) 283.
[24] F.L. Eisele, D.J. Tanner, J. Geophys. Res. 96 (1991) 9295.
[25] F.L. Eisele, J. Geophys. Res. 91 (1986) 7897.
[26] A.A. Viggiano, J.V. Seeley, P.L. Mundis, J.S. Williamson, R.A. Morris, J. Chem. Phys. A 101 (1997) 8275.
[27] A.A. Viggiano, R.A. Perry, D.L. Albritton, E.E. Ferguson, F.C. Fehsenfeld, J. Geophys. Res. 87 (1982) 7340.
[28] W.B. DeMore, S.P. Sander, D.M. Golden, R.F. Hampson, M.J. Kurylo, C.J. Howard, A.R. Ravishankara, C.E. Kolb, M.J. Molina, Chemical Kinetics and Photochemical Data for Use in Stratospheric Modeling, JPL Publ. 97-4, Pasadena, 1997.
[29] A.A. Viggiano, F. Arnold, in H. Volland (Ed.), Handbook of Atmospheric Electrodynamics, I, CRC, Boca Raton, 1995, p. 1.
[30] C.A. Cantrell, A. Zimmer, G.S. Tyndall, Geophys. Res. Lett. 24 (1997) 2195.
[31] D. Poppe, R. Bauer, T. Brauers, D. Brüning, J. Callies, H.P. Dorn, A. Hofzumahaus, F.J. Johnen, A. Khedim, R. Koppmann, H. London, K.P. Müller, R. Neuroth, C. Plass-Dülmer, U. Platt, F. Rohrer, J. Rudolph, U. Schmidt, A. Wahner, M. Wallasch, M. Weber, D. Ehhalt, J. Geophys. Res. 99 (1994) 16 633.
[32] O. Möhler, T. Reiner, F. Arnold, Rev. Sci. Instrum. 64 (1993) 1199.